HHS Public Access

Author manuscript

Nat Med. Author manuscript; available in PMC 2014 September 01.

Published in final edited form as:

Nat Med. 2014 March ; 20(3): 255–264. doi:10.1038/nm.3464.

Rejuvenation of the aged muscle stem cell population restores strength to injured aged muscles

Benjamin D. Cosgrove[1], **Penney M. Gilbert**[1,2,*], **Ermelinda Porpiglia**[1], **Foteini Mourkioti**[1], **Steven P. Lee**[1,3], **Stephane Y. Corbel**[1], **Michael E. Llewellyn**[3], **Scott L. Delp**[3,4], and **Helen M. Blau**[1,*]

[1]Baxter Laboratory for Stem Cell Biology, Department of Microbiology and Immunology, and Institute for Stem Cell Biology and Regenerative Medicine, Stanford University School of Medicine, Stanford, CA, USA

[2]Institute of Biomaterials and Biomedical Engineering and Donnelly Centre for Cellular and Biomolecular Research, University of Toronto, Toronto, Ontario, Canada

[3]Department of Bioengineering, Stanford University School of Medicine, CA, USA

[4]Department of Mechanical Engineering, Stanford University School of Medicine, CA, USA

Abstract

The aged suffer from progressive muscle weakness and regenerative failure. We demonstrate that muscle regeneration is impaired with aging due in part to a cell-autonomous functional decline in skeletal muscle stem cells (MuSCs). Two-thirds of aged MuSCs are intrinsically defective relative to young MuSCs, with reduced capacity to repair myofibers and repopulate the stem cell reservoir *in vivo* following transplantation due to a higher incidence of cells that express senescence markers and that have elevated p38α/β MAPK activity. We show that these limitations cannot be overcome by transplantation into the microenvironment of young recipient muscles. In contrast, subjecting the aged MuSC population to transient inhibition of p38α/β in conjunction with culture on soft hydrogel substrates rapidly expands the residual functional aged MuSC population, rejuvenating its potential for regeneration, serial transplantation, and strengthening damaged muscles of aged mice. These findings reveal a synergy between biophysical and biochemical cues that provides a paradigm for a localized autologous muscle stem cell therapy in aged individuals.

[*]**Corresponding authors**: Helen M. Blau, Ph.D., Baxter Laboratory for Stem Cell Biology, Stanford University School of Medicine, 269 Campus Drive, CCSR 4215, Stanford, CA 94305, USA, Tel: 650-723-6209 / hblau@stanford.edu, Penney M. Gilbert, Ph.D., Institute of Biomaterials and Biomedical Engineering, University of Toronto, 160 College Street, Room 510, Toronto, Ontario M5S 3E1, Canada, Tel: 416-978-2501 / penney.gilbert@utoronto.ca.

AUTHOR CONTRIBUTIONS

B.D.C., P.M.G., and E.P. designed and performed experiments, analyzed data, and wrote the manuscript. F.M., S.P.L., S.Y.C., and M.E.L. developed methods, performed experiments, and analyzed data. S.L.D. developed methods and wrote the manuscript. H.M.B. designed experiments, analyzed data, and wrote the manuscript.

COMPETING FINANCIAL INTERESTS

The authors have no competing interests as defined by Nature Publishing Group, or other interests that might be perceived to influence the results and/or discussion reported in this article.

INTRODUCTION

During aging, skeletal muscle strength progressively declines (sarcopenia), leading to reduced mobility, function, and quality of life[1,2]. A number of pharmacologic strategies to treat muscle wasting have been proposed that are directed at reversing myofiber atrophy or promoting myofiber hypertrophy and are largely designed to target mitochondrial, catabolic, and anabolic mechanisms in the context of cachexia or sarcopenia[3–6]. Despite these major advances, no pharmacologic therapies are currently in clinical use that ameliorate or reverse the decline in muscle strength in the aged[7,8], which constitutes a costly and ever-increasing health-care concern[9].

An alternative or synergistic strategy for increasing muscle strength enlists the regenerative capacity of muscle stem cells (MuSCs; also known as satellite cells[10]) that reside on muscle fibers and are dedicated to their repair. Since MuSC numbers remain relatively constant during aging in mice and humans until late in life, a reduced stem cell abundance does not fully account for the impaired regeneration observed during aging[11]. Instead, several reports attribute loss of muscle regenerative capacity to changes in the aged systemic and local microenvironments, not to the stem cells themselves[2,12–16]. For example, systemic factors from young mice ameliorate muscle regeneration in aged mice following heterochronic parabiosis[13,15]. In addition, targeting microenvironmental factors characteristic of aged muscle tissues, such as signalling via the Wnt, bFGF and Notch pathways, enhances regeneration[13,14,17].

Here we show that the MuSC population from aged mice is inherently defective in its essential functions of regenerating damaged myofibers and repopulating the stem cell reserve. We demonstrate that the reduced function of aged MuSCs can be overcome in culture by the combined effects of a small molecule inhibitor of p38α/β MAPK and a porous hydrogel substrate with biophysical properties matching the soft elasticity of muscle tissue. The synergistic combination of these biochemical and biophysical cues stimulates the rapid expansion of functional stem cells within the aged MuSC progeny to generate a stem cell population with rejuvenated function capable of restoring strength to injured aged muscles.

RESULTS

Aged MuSCs exhibit cell-autonomous muscle regeneration defects

Transplantation of purified muscle stem cells in conjunction with a sensitive imaging assay of engraftment, a measure of regeneration, first revealed that aged MuSCs are intrinsically two-thirds less effective than young MuSCs in regenerating muscle (Fig. 1). A major advance in the muscle field is that MuSCs can now be prospectively isolated from mice to high purity by fluorescence activated cell sorting (FACS)[18–23]. We isolated and enriched MuSCs from young and aged mice (2 and 24 months, respectively) by FACS for $CD45^{-}CD31^{-}CD11b^{-}Sca1^{-}CD34^{+}\alpha7\text{-integrin}^{+}$ cells to ≥95% purity, as previously described[23] (Supplementary Fig. 1a). We employed limiting dilution analysis, a classic assay in the hematopoiesis field[24] to quantify and compare the frequency of cells with stem cell function within heterogeneous, prospectively isolated populations. We injected different numbers (10, 20, 100, or 300 cells) of young or aged MuSCs freshly isolated from

transgenic *GFP*/*Luciferase* mice intramuscularly into irradiated hindlimb muscles of young NOD/SCID mice (Fig. 1a–f). Transplant engraftment was monitored *in vivo* by bioluminescence imaging (BLI) and confirmed by retrospective GFP immunohistochemistry[23]. BLI is well suited to an analysis of low numbers of transplanted luciferase-expressing MuSCs as it can sensitively capture the engraftment and dynamic expansion of an initially undetectable small population of cells (Supplementary Fig. 1b). BLI correlates well with traditional immunohistochemical measures of contribution to myofibers (Supplementary Fig. 1c). No difference in engraftment frequency was seen upon transplantation of 100 or more cells (Fig. 1f), in agreement with previous findings by others[16]. However, when we delivered as few as 10 cells, a difference was revealed and aged MuSC transplants engrafted at a markedly reduced frequency relative to young. Both the fraction of transplants that engrafted and the number of GFP^+ myofibers observed in engrafted recipients were lower (Fig. 1b–f). Although the analyses presented throughout this study focused on female donor MuSCs, we observed similar results with male donor MuSCs (Supplementary Fig. 1d). Analysis of the transplant results using a stem cell limiting dilution model[24] revealed that aged MuSCs exhibited a two-thirds reduction in engraftment capacity compared to young MuSCs (Fig. 1f and Supplementary Fig. 1e). Thus, this sensitive and quantitative assay revealed that, even in the microenvironment of young muscles, the proportion of the aged MuSC population with repair function was greatly reduced relative to young, due to a cell-autonomous defect.

Aged MuSCs are defective in repopulation and serial transplantation

The most exacting measure of long-term MuSC potential is serial transplantation, the ability of MuSCs to regenerate tissues in successive recipients[25,26]. We established a serial transplantation assay to compare long-term function of young and aged *GFP*/*Luciferase* MuSCs (Fig. 1a). First, we evaluated stem-cell repopulation in primary recipients by flow cytometric detection of donor-derived (GFP^+) MuSCs as a fraction of the total recipient MuSC ($CD34^+\alpha7\text{-integrin}^+$) population after transplantation (Fig. 1g). In order to compare stem-cell repopulation potential between young and aged MuSCs, we performed transplants with a range of cell numbers (100, 200, and 700 cells) enabling a comparative limiting dilution analysis. Aged MuSCs gave rise to a substantially smaller fraction of the total MuSC population in primary recipients than did young MuSCs (Fig. 1h and Supplementary Fig. 2a). These results provide further evidence for a cell-autonomous stem cell self-renewal defect in two-thirds of aged MuSCs.

The entire population of GFP^+ MuSCs isolated from primary recipient muscles was immediately transplanted into secondary recipient muscles. We compared only the GFP^+ ($CD34^+\alpha7\text{-integrin}^+$) MuSC population (Supplementary Fig. 2b,c) and used a relatively high number of MuSCs (700 cells) in the primary transplants to ensure that sufficient numbers could be re-isolated for secondary transplants. Relative to young, aged secondary donor MuSCs exhibited significantly reduced engraftment in secondary recipients (Fig. 1i,j and Supplementary Fig. 2c). These findings demonstrate that the regenerative capacity of serially transplanted aged MuSCs is diminished relative to young, in agreement with findings for aged hematopoietic stem cells[27]. Notably, these results confirm that the intrinsic defects in aged MuSCs are not corrected upon transplantation into a young muscle tissue

environment and that only a subset of the aged population retains the long-term functional capacity to reconstitute the stem-cell reservoir *in vivo*.

Molecular and cellular changes are evident in aged MuSCs

We sought to identify molecular defects in aged MuSCs that could be targeted therapeutically to enhance their function. We assayed single MuSCs by nested reverse transcriptase-polymerase chain reaction (RT-PCR)[23] for their expression of signature MuSC genes[28,29] which showed they were similarly highly enriched for *Pax7*$^{+}$*Myod* stem cells (Fig. 2a and Supplementary Fig. 3a). The expression of these markers showed that the diminished function was not attributable to differences in the purity of the isolated cell population. A conundrum in propagating adult MuSCs *ex vivo* is that MuSCs rapidly lose their stem cell function when cultured on standard tissue culture plastic (10^6 kPa rigidity)[20,23,30,31]. We previously showed that this problem can be overcome and stem cell function retained if MuSCs are maintained on soft, porous hydrogel substrates with a rigidity (12 kPa) similar to skeletal muscle tissue and conjugated with the MuSC niche protein laminin[30]. We compared the clonal cell division capacity of young and aged MuSCs in hydrogel microwells and observed that, relative to young MuSCs (18%), a higher proportion of aged MuSCs (33%) were unable to divide in mitogenic medium (Fig. 2b,c), in accordance with previous findings using other culture systems[32–35] and those evaluating aged human myoblasts[36]. This decrease in the proliferative potential of aged MuSCs was not due to differential survival, as no difference in the viability of young and aged MuSCs was observed (Supplementary Fig. 3b).

Hallmarks of aging-associated cell senescence[27] were elevated, as shown by immunocytochemical analyses of the cell cycle inhibitors $p16^{Ink4a}$ and $p21^{Cip1}$ in freshly FACS purified aged MuSCs (19%) relative to young MuSCs (0.3%) (Fig. 2d,e). Expression of these senescence factors can be induced by persistent activation of cellular stress-related pathways[37–39]. By assaying stress signaling pathways by phosphoprotein flow cytometric analysis, we found that greater proportions of aged MuSCs (25%), relative to young (2%), exhibited active p38α/β mitogen-activated protein kinase (MAPK) signaling (Fig. 2f,g). These data revealed aberrant p38α/β MAPK signaling as a potential therapeutic target in aged MuSCs.

p38α/β inhibition enhances aged MuSC proliferation

We postulated that inhibiting p38α/β signaling during culture of aged MuSCs on soft hydrogel substrates could enhance their stem-cell function. After one week on soft hydrogel substrates, elevated p38α/β signaling activity persisted in aged relative to young MuSC cultures (Fig. 3a,b). Treatment of aged MuSC cultures with SB202190 (hereon, abbreviated SB), an imidazole-based ATP competitive inhibitor of the α and β isoforms of p38 MAPK, substantially reduced p38α/β signaling to levels below those of cultured young MuSCs in a dose-dependent fashion with saturated effect by 25 μM (Fig. 3b). By contrast, JNK signaling, a previously reported off-target of SB in some cell types[40], was not affected. To confirm the SB effects, we transiently knocked down p38α and p38β with isoform-specific siRNAs (Supplementary Fig. 4a,b). When we delivered the two siRNAs together, efficacious knockdown of both p38α and p38β expression was achieved (Supplementary

Fig. 4c,d). The combined p38α/β siRNA treatment demonstrated a decrease in phospho-HSP27^{+} cell frequency in aged MuSC cultures, providing further confirmation of SB's target (Fig. 3a,b).

Transient (one-week) SB treatment alleviated the proliferative defect in aged MuSCs in a concentration-dependent manner (Fig. 3c and Supplementary Fig. 5). A one-week SB treatment of aged MuSCs yielded a 35-fold increase in cumulative cell number relative to the starting population, and a similar change in cell number was also observed for SB-treated young MuSCs. The proliferative enhancement due to p38α/β inhibition was more pronounced for aged than young MuSCs when compared to their respective uninhibited conditions (18-fold and 11-fold higher, respectively; Supplementary Fig. 5a,b). A similar enhancement in aged MuSC proliferation was also observed by combined p38α/β siRNA treatment (Fig. 3c). The proliferative effect was maximal at 10 μM SB, with a reduced effect observed at 25 μM, as previously reported[41] (Supplementary Fig. 5c); therefore, a 10 μM concentration was used for all following studies.

In parallel with the marked increase in proliferation and total cell number, the proportion of both non-dividing cells was and p16^{Ink4a}-expressing cells was lower in the aged MuSC population upon SB treatment (Fig. 3d–f). Notably, these changes were not evident for SB-treated young MuSCs. Thus, SB treatment minimizes the incidence of cell-cycle arrested (quiescent and senescent) cells within the aged MuSC culture progeny.

p38α/β inhibition and hydrogel synergistically affect aged MuSC fates

To determine if the molecular phenotype of SB and hydrogel-treated aged MuSCs was altered in a synergistic manner, we examined expression signatures of muscle stem cells and committed progenitors at the transcriptional and protein levels. Treatment of aged MuSCs with either the SB inhibitor or the combined p38α/β siRNAs yielded increased expression of the muscle stem cell marker *Pax7* and decreased expression of the commitment marker *Myogenin*, as measured by RT-qPCR, but only when maintained on soft hydrogels (Fig. 3g,h). Moreover, single-cell RT-PCR and protein flow cytometry assays confirmed that expression of these markers is inversely correlated and that SB treatment promotes a shift in the aged cell population towards a higher incidence of Pax7^{+}Myog^{-} stem cells and fewer Pax7^{-}Myog^{+} committed progenitors (Supplementary Fig. 6). *Pax7* muscle stem cell marker expression was not markedly enhanced for SB-treated young MuSCs on hydrogel, suggesting the effect of substrate rigidity was predominant and sufficed (Fig. 3g). By contrast, aged MuSCs on hydrogel alone or with SB treatment alone did not exhibit enhanced *Pax7* expression, but required the synergistic interaction of the biophysical and biochemical cues.

A recent report[42] demonstrated that MuSC self-renewal divisions are associated with an asymmetric distribution of active p38α/β signaling components into more committed progeny cells. In accordance with those findings, we observed that the committed progenitors in the aged MuSC progeny are those with elevated p38α/β signaling activity (Fig. 3i). Taken together, these observations show aged MuSCs require synergistic biophysical (hydrogel substrate) and biochemical (p38α/β inhibitor) cues in order to augment stem cell gene expression (Fig. 3j).

Regenerative potential of aged MuSC populations is restored

To determine if the synergistic effects of p38α/β inhibition and soft hydrogel substrates that led to stem cell marker expression *ex vivo* also altered stem cell function *in vivo*, we tested the regenerative capacity of treated young and aged MuSC populations after transient culture. We exposed young or aged MuSC populations to diverse culture conditions for one-week and then transplanted equivalent numbers (100 cells) into mice to directly compare the proportion of cells with stem-cell regenerative capacity as assessed by BLI and analyzed using the limiting dilution model (Fig. 4a–c and Supplementary Fig. 7). On hydrogel alone, a substantial difference was observed between young (34% transplants engrafted) and aged (5%) MuSC culture populations (Fig. 4b,c). Although SB exposure did not significantly alter young MuSC engraftment (45%), SB significantly enhanced aged MuSC engraftment (41%) to a level similar to young MuSC populations in hydrogel culture alone. These findings were confirmed using an alternate p38α/β inhibitor, BIRB0796 (Supplementary Fig. 7a). Thus, the combination of biophysical and biochemical cues raised the proportion of MuSCs with regenerative function within the aged population to be equivalent to that of the young MuSC population in culture (Supplementary Fig. 7b), resulting in a rejuvenated population.

Yield of functional stem cells from aged muscles is increased

Given the greatly enhanced proportion of MuSCs with proliferative (Fig. 3c,d) and regenerative capacity observed (Fig. 4b,c), we asked whether the synergistic SB/hydrogel condition yielded a cumulative number of functional stem cells in culture that exceeded that of the freshly purified, uncultured aged MuSC population. Such a result would demonstrate expansion of the functional population had occurred *ex vivo*. We predicted the extent of *ex vivo* expansion by combining the proliferation and limiting dilution engraftment analyses and estimated that SB/hydrogel treatment induces an average 6-fold (95% confidence interval range: 3–17 fold) increase in functional stem cell numbers in the aged population (Supplementary Fig. 7b). To test this possibility, we compared equal numbers (10 cells) of young freshly isolated and aged freshly isolated MuSCs to the progeny of 10 aged MuSCs after one-week of SB/hydrogel culture (a yield of 270 total cells) in transplantation assays (Fig. 4d,e). Freshly isolated aged MuSCs resulted in a 33% transplant engraftment, whereas the SB/hydrogel culture progeny resulted in 79% engraftment, similar to freshly isolated young MuSCs (63%; Fig. 4f). The improved transplant engraftment frequency of the aged SB/hydrogel progeny provides evidence of a rapid expansion of the functional stem cell population.

p38α/β inhibition enhances clonal expansion of aged MuSCs

To determine the basis for the stem-cell expansion of the aged MuSC population, we performed single-cell fate analyses of aged MuSCs, which is critical given the inherent heterogeneity in MuSC populations[16,19,20,23,25,30]. We established a clonal stem cell-fate assay by culturing single MuSCs in hydrogel “microwells” and analyzing their proliferative behavior by long-term time-lapse microscopy using the automated Baxter cell tracking and lineage reconstruction algorithm[30] paired with an immunocytochemical assay of myogenic differentiation (Fig. 4g–i). This single-cell analysis revealed that not only did SB treatment enhance the number of aged MuSCs that gave rise to clones (Fig. 3d), but it also led to a

marked increase in the number of cells per aged MuSC clone. Furthermore, SB treatment significantly prevented myogenic differentiation assessed by Myogenin expression, indicative of a clonal expansion in Myogenin$^-$ uncommitted stem and progenitor cells (Fig. 4h,i). Together, these single-cell observations and *in vivo* functional data (Fig. 4d–f) indicate that the SB/hydrogel treatment synergizes to stimulate extensive proliferation without differentiation, suggesting that aged MuSC expansion occurs by self-renewal.

Expanded aged MuSC population has enhanced long-term function

Repeated capacity to regenerate tissue is an essential characteristic of long-term stem cell function[23,31], which we observed to be defective in aged MuSCs compared to young (Fig. 1g–j and Supplementary Fig. 2c). The reconstitution of the functional stem cell reserve *in vivo* by 200 freshly isolated aged *GFP*/*Luciferase* MuSCs or their hydrogel culture progeny ± SB treatment was compared by flow cytometric, immunohistochemical, and serial transplant assays (Fig. 5a–f). We re-isolated and quantified GFP$^+$ MuSCs from the muscles of primary recipient mice (Fig. 5b) and transplanted them into secondary recipients (Fig. 5d–f). We observed that the SB/hydrogel progeny transplants resulted in an enhanced stem cell reconstitution as evidenced by a greater proportion of donor-derived (median 21% GFP$^+$) MuSCs in primary transplant recipients, compared to freshly isolated aged MuSCs (5% GFP$^+$) or the progeny from hydrogel-only culture transplants (0% GFP$^+$; Fig. 5b). Histological analysis confirmed that MuSCs from aged *Myf5*$^{LacZ/+}$ transgenic mice[43] expanded *ex vivo* by SB/hydrogel treatment home to the native satellite cell niche one month following transplantation to replenish the long-term stem cell reserve (Fig. 5c). Moreover, these cells are capable of responding to subsequent regenerative demands in transplant recipients, as evidenced by the activation of Myf5 expression upon notexin damage[20,23,30,43].

Furthermore, compared to fresh aged MuSCs, which have diminished capacity to regenerate muscles upon serial transplant (see Fig. 1i,j), the progeny of aged MuSCs from SB/hydrogel cultures can be serially transplanted yielding robust and stable engraftment and GFP$^+$ myofibers in secondary recipients (Fig. 5d–f). Thus, the aged MuSC population from SB-treated hydrogel cultures overcomes the defect in long-term cell re-population seen with freshly isolated aged cells providing further evidence of *ex vivo* expansion of the functional stem cell population.

Rejuvenated aged MuSC population restores strength to aged muscles

We developed a preclinical model of autologous cell therapy to evaluate whether SB-treated aged MuSC populations could regenerate the injured muscles of aged mice. The experiments described above (Figs. 1, 4 and 5) all used immunocompromised young NOD/SCID recipients. In contrast, here we evaluated aged MuSCs transplanted into syngeneic, age-matched C57BL/6 wild-type recipients two days following local notexin injury (Fig. 6a). We compared the soft hydrogel-culture progeny of 200 aged MuSCs (without or with SB treatment, which proliferated extensively to yield 740 and 13,000 total cells per transplant respectively; Fig. 6b). We infected cells with a *Luciferase*-IRES-*GFP* lentivirus for engraftment analyses. Transplants of SB-treated aged MuSC progeny engrafted at a higher frequency in aged wildtype than in young NOD/SCID mice (90%), whereas hydrogel-only

aged MuSC progeny did not (0%; Fig. 6c). Moreover, the transplanted SB progeny contributed to the repair of a high proportion (63%; Fig. 6d,e) of recipient myofibers, as assessed by Luciferase immunohistochemistry, which is likely a substantial under-representation given that using the lentiviral approach, only 33% of cells were labeled with the transgene pre-transplantation (Supplementary Fig. 8a). These data suggest that the expanded aged MuSC population had increased to a number that was effective in repairing the majority of myofibers in injured aged muscles.

As the ultimate test of functional recovery, we determined whether the delivery of *ex vivo* SB-treated aged MuSC progeny could restore muscle strength to notexin-injured aged recipients one month post-transplant. To avoid potential artifacts associated with measurements that entail complete muscle excision and rigor mortis, we assayed specific twitch and tetanus force generation in intact *tibialis anterior* muscles in live anesthetized mice[44,45] (Fig. 6f). Compared to muscles of young mice, muscles of aged mice exhibited reduced twitch forces, while tetanus forces were similar (Fig. 6g,h and Supplementary Fig. 8b–d). These observations are in agreement with prior reports that a reduction in fast-twitch (type II) rather than slow-twitch (type I) fibers is observed with aging[46]. Injured muscles of aged mice exhibited defective regeneration, evident by both impaired twitch and tetanus force generation, as expected[2]. Transplantation of freshly isolated aged MuSCs resulted in a minor recovery in twitch force. By contrast, injured aged muscles that received transplants of the hydrogel/SB-treated aged MuSC progeny exhibited increases in both twitch and tetanus forces that were restored to the levels of uninjured young muscles. The cell numbers required are consistent with a recent report that 900 or more young functional MuSCs are necessary and sufficient to achieve *tibialis anterior* strength recovery in a dystrophic mouse model[47]. Our findings provide evidence of the potent restorative function of the expanded aged MuSC population, even in an aged injured syngeneic and immunocompetent recipient.

DISCUSSION

Here we present novel evidence that aged MuSCs differ intrinsically from young MuSCs and provide a strategy to rejuvenate the function of aged MuSC populations *ex vivo*. We demonstrate that aged MuSCs have cell-autonomous self-renewal defects that lead to impaired regeneration, stem-cell repopulation, and serial transplantation *in vivo*, which are not corrected even when transplanted into young mice. These findings show that in addition to previously described marked effects of extrinsic systemic and tissue microenvironmental changes[13,15], factors intrinsic to MuSCs also change and impair muscle regeneration with aging. Given the rarity of stem cells in muscle tissues, the determination that stem cell populations from aged muscles have lost two-thirds of the functional capacity of those from young muscles constitutes a major challenge for stem cell-based therapies in the aged. However, this observation also provides a previously unrecognized opportunity to identify cell-intrinsic molecular changes in the aged population that can be targeted to increase the number of fully functional stem cells, in order to realize the goal of an autologous stem cell therapy for the aged.

We show that a greater proportion of muscle stem cells from aged muscles exhibit persistently elevated p38α/β MAPK activity and expression of the cell-cycle inhibitors

p16^{Ink4a} and p21 compared to young MuSCs. p38α/β signaling inhibits muscle stem cell gene expression, promotes myoblast differentiation, and is required for muscle regeneration[41,42,48,4950]. In agreement with our findings in muscle, p38α/β signaling has been reported to induce p16^{Ink4a} expression and promote cell senescence in human fibroblasts[39] and its inhibition can extend the proliferative lifespan of fibroblasts[51], pancreatic islet cells[37], and hematopoietic stem cells[38,52]. Others have noted that activated satellite cells retain phosphorylated p38α/β[42] and aged satellite cells have a more "activated" phenotype *in vivo*[17]. Here we extend these findings by showing that aged MuSCs manifest an intrinsic difference in p38α/β signaling.

We show that the synergistic action of both a biophysical cue (substrate rigidity) as well as a biochemical cue (p38α/β signaling inhibitor) is required to rejuvenate the cumulative aged MuSC population. Neither of these factors alone is efficacious in enhancing aged MuSC *Pax7* expression and transplant engraftment. In contrast, the biophysical cue of substrate rigidity predominates for young MuSCs, as might be expected given their minimal p38α/β activity. Thus, the observed synergistic effects on *ex vivo* self-renewal are specific to aged MuSCs.

Our findings demonstrate that active p38α/β is a potent target for directed and rapid expansion of functional stem cells from aged muscle tissues, when administered in the context of soft hydrogel. The SB/hydrogel progeny had improved function over the freshly isolated aged stem cells, evidence of *ex vivo* expansion of the residual 33% of functional MuSCs. Importantly, this *ex vivo*-expanded aged MuSC population conferred long-term beneficial effects *in vivo* in mice, as the cells exhibited enhanced repopulation of the stem cell reservoir and function in serial transplants. To our knowledge, this is the first strategy reported for rapid and directed functional stem cell expansion from aged muscle tissues. Notably, the expanded aged MuSC population contributed to extensive myofiber repair and restored strength to injured aged muscles.

Adult stem cells are advantageous for regenerative medicine as they have a known identity, integrate well within the tissue following delivery, and are committed to regenerating their tissue of origin. Moreover, their potential for tumorigenicity is low, as skeletal muscle tumors (rhabdomyosarcoma) are very rare in adults[53]. Treatment *ex vivo* avoids possible side effects within other tissues that could result when small molecule inhibitors[54] or siRNAs are delivered systemically. Our findings provide a paradigm for rapid, marked expansion of functional MuSCs *ex vivo* by short-term treatment in culture leading to an autologous muscle stem cell therapy for restoring strength in cases of localized muscle damage in aged individuals.

ONLINE METHODS

Animals

The Stanford University Administrative Panel on Laboratory Animal Care (APLAC) approved all animal protocols. We performed all experiments in compliance with the institutional guidelines of Stanford University. We purchased C57BL/6 mice from US National Institute of Aging. We generated mice ubiquitously expressing a green fluorescent

protein (*GFP*) transgene, mice ubiquitously expressing a firefly luciferase (*Fluc*) transgene driven by the *ACTB* promoter (L2G85 strain), and mice expressing *nLacZ* under regulation of the *Myf5* promoter (*Myf5*$^{nLacZ/+}$)[43] as described previously[23]. We generated double transgenic *GFP*/*Luciferase* and *Myf5*$^{nLacZ/+}$/*Luciferase* mice by breeding the above strains. We validated these genotypes by appropriate PCR-based strategies. We used cells from C57BL/6 mice for cell proliferation, phosphoprotein analysis, gene expression and syngeneic transplant experiments. We used cells from *GFP*/*Luciferase* and *Myf5*$^{nLacZ/+}$/*Luciferase* mice for allogenic transplantation experiments into NOD/SCID (Jackson Laboratory) recipient mice. We studied young mice at 2–4 months of age (median 2 months) and aged mice at 22–28 months of age (median 24 months) for all strains and genders. All mice used in these studies were females, except as noted in Supplementary Fig. 1d.

Muscle stem cell (MuSC) isolation

We isolated and enriched muscle stem as previously described[23]. Briefly, we dissected *tibialis anterior* and *gastrocnemius* muscles from mice and subjected them to collagenase (0.25%; Roche) and dispase (0.04 U ml^{-1}; Roche) digestion. After this digestion step, we kept cells at 4 °C until culture or transplantation. We removed non-muscle tissue under a dissection microscope and then dissociated muscle fibers. After 90 min total digestion, we passed the remaining cell suspension through sequential 70-μm and 40-μm filters (BD Biosciences) to generate single-cell suspensions. We first incubated cells with biotinylated antibodies reactive to CD45 (BD Biosciences, clone 30F11, catalog # 553078, 1:500), CD11b (BD Biosciences, clone M1/70, catalog # 553309, 1:800), CD31 (eBiosciences, clone 390, catalog # 13-0311-82, 1:200), and Sca1 (BD Biosciences, clone E13-161.7, catalog # 553334, 1:200). We then incubated cells with streptavidin magnetic beads (Miltenyi Biotech), streptavidin-Texas Red (Invitrogen, catalog # S872, 1:200), α7-integrin-phycoerythrin antibody (AbLab, clone R2F2, catalog # 10ST215, 1:500), and CD34-eFluor660 antibody (eBioscience, clone RAM34, catalog # 50-0341-82, 1:67).

We magnetic depleted biotin-positive cells on a selection column (Miltenyl). We then sorted the biotin-negative cells on a modified FACStar Plus or FACS Aria cell sorter using FACS Diva software (BD Biosciences). We enriched MuSCs by gating viable cells (propidium iodide-negative) for cells negative for the lineage marker panel (CD45, CD31, CD11b, and Sca1) and positive for both CD34 and α7-integrin. We double-sorted cells for purity (routinely >95% for cells from C57BL/6 mice). For cells from *GFP*/*Luciferase* mice, we also gated for GFP positivity and routinely obtained >92% double-sorted purity. We generated and analyzed flow cytometry scatter plots using FlowJo v8.7 (Treestar).

MuSC transplantation

We transplanted MuSCs immediately following FACS isolation or after collection from cell culture directly into the *tibialis anterior* muscle of recipient mice as previously described[23,30]. We transplanted cells from *GFP*/*Luciferase* or *Myf5*$^{nLacZ/+}$/*Luciferase* mice into gender-matched, hindlimb-irradiated NOD/SCID mice (Figs. 1, 4, and 5). Before transplantation, we anesthetized NOD/SCID mice (2–4 months of age, median 2 months) with ketamine (2.4 mg per mouse) and xylazine (240 μg per mouse) by intraperitoneal

injection. We then irradiated hindlimbs by a single 18 Gy dose, with the rest of the body was shielded in a lead jig. We performed transplantations within three days of irradiation.

In syngeneic studies (Fig. 6), we transplanted cells from aged C57BL/6 mice into non-irradiated, gender-matched, littermate aged C57BL/6 mice (Jackson). For these experiments, aged C57BL/6 MuSCs were exposed to a *Luciferase*-IRES-*GFP* lentivirus at day 2 of culture for a period of 24 h. Two days prior to cell transplantation, we acutely injured *tibialis anterior* muscles in recipient aged C57BL/6 mice by a single 10 μl intramuscular injection of notexin (10 μg ml^{-1}; Latoxan).

We collected cells from hydrogel cultures by incubation with 0.5% trypsin in PBS for 2 min at 37 °C. and counted using a hemocytometer. For both FACS isolated and cultured cells, we washed cells three times and counted them with a hemocytometer. We resuspended cells at desired cell concentrations in PBS with 2.5% goat serum and 1 mM EDTA and then transplanted them by intramuscular injection into the *tibialis anterior* muscles in a 10 μl volume. We compared cells from different conditions by transplantation into the *tibialis anterior* muscles of contralateral legs in the same mice.

Bioluminescence imaging

We performed bioluminescence imaging (BLI) using a Xenogen-100 system, as previously described[23]. Briefly, we anesthetized mice using isoflurane and administered 100 μL D-luciferin (0.1 mmol kg^{-1}, reconstituted in PBS; Caliper LifeSciences) by intraperitoneal injection. We analyzed BLI using a 60 s exposure acquired at 12 min after luciferin injection. Digital images were recorded and analyzed using Living Image software (Caliper LifeSciences). We analyzed images with a consistent region-of-interest (ROI) placed over each hindlimb to calculate a bioluminescence signal. We used a bioluminescence signal value of 80,000 photons s^{-1} to define an engraftment threshold. This BLI level corresponds to the histological detection of one or more GFP^+ myofibers (see Supplementary Fig. 1c and also[30]). We performed BLI imaging at one month after transplantation, unless otherwise stated.

Tissue histology

We collected and prepared recipient *tibialis anterior* muscle tissues for histology to analyze the expression of donor-cell transgene products as previously described[23]. We incubated transverse sections with anti-Laminin (Millipore, clone A5, catalog # 05-206, 1:250), anti-GFP (Invitrogen, catalog # A11122, 1:200), and/or anti-Luciferase (Abcam, catalog # ab81822, 1:100) primary antibodies and then with appropriate secondary antibodies (Invitrogen). We counter-stained nuclei with Hoechst 33342 (Invitrogen) or Topro3 (Invitrogen). We acquired images with an AxioPlan2 epi-fluorescent microscope (Carl Zeiss Microimaging, Thornwood, NY) with Plan NeoFluar 10x/0.30NA or 20x/0.75NA objectives (Carl Zeiss) and an ORCA-ER digital camera (Hamamatsu Photonics). We captured digital images in OpenLab software (Improvision) and assembled multi-panel figures using Photoshop software (Adobe) with consistent contrast adjustments across all images from the same stain.

Limiting dilution analysis

To calculate the effective number of functional MuSCs in any transplanted cell population, We related the transplant engraftment efficiency to the number of cells transplanted (across a range of transplanted cell numbers) using an exponential stem-cell limiting dilution model[24]:

$$\%\text{engraftment} = 100\% \cdot [1 - \exp[-(\beta_{\text{sample}}) \cdot (\#\text{cells transplanted}_{\text{sample}})]] \quad \text{[eqn. 1]}$$

where β is an exponential coefficient fit from experimental data. This model fit well to experimental data from young and aged MuSC transplants (R^2 = 0.92–0.99, range; see Fig. 1f and Supplementary Figs. 1e and 7b). Using this model, we calculated the absolute number of "functional" MuSCs (defined as equivalent to freshly isolated young MuSCs) within any given population using:

$$\#\text{FunctionalMuSCs}_{\text{sample}} = (\beta_{\text{Sample}} / \beta_{\text{Yng,Fresh}}) \cdot (\#\text{cells}_{\text{sample}}). \quad \text{[eqn. 2]}$$

Serial transplantation assay

We transplanted a set number (e.g., 700 in Fig. 1i,j and 200 in Fig. 5d–f) of freshly isolated MuSCs or a one-week culture progeny from the same starting number of cells into hindlimb-irradiated NOD/SCID primary recipients. One month after transplant, we collected and digested primary recipient muscles. We re-isolated donor cells by gating for cells negative for propidium iodide and the CD45/CD11b/CD31/Sca1 lineage markers and positive for the donor GFP markers from primary recipient muscle cell digestion by FACS. We gated the GFP^+ cells into two populations by FACS based on their expression of the $CD34^+\alpha7\text{-integrin}^+$ MuSC surface marker signature. See Supplementary Fig. 2b for representative FACS scatter plots for re-isolation sorting. To performed secondary transplants, we pooled cells isolated from multiple primary recipients that received cells from the same condition and distributed them equally amongst each secondary transplant recipient such that the average yield of GFP^+ MuSCs collected from each primary transplant recipient was injected into each secondary recipient. One month later, we analyzed these secondary recipients by BLI for transplant engraftment.

Quantification of donor-derived MuSCs in transplant recipients

We used flow cytometric to quantify donor-derived (GFP^+) MuSCs as a proportion of all $CD34^+\alpha7\text{-integrin}^+$ MuSCs in recipient muscles after transplantation with freshly isolated *GFP*/*Luciferase* MuSCs or their culture progeny. One-month post-transplant, we assessed transplant engraftment by bioluminescence imaging. The following day, we collected and digested primary transplant recipient *tibialis anterior* muscles. We labelled and magnetically depleted cell suspensions based on CD45, CD11b, CD31, and Sca1 expression. From this depleted population, we gated cells negative for propidium iodide and CD45/CD11b/CD31/Sca1 gated by FACS. Within this population, we analyzed $CD34^+\alpha7\text{-integrin}^+$ cells, representing the entire recipient MuSC population, for GFP positivity (see Fig. 1g).

Single-cell RT-PCR

We performed nested multiplexed RT-PCR on freshly sorted single MuSCs or single cells from harvested culture to evaluate muscle stem and progenitor cell phenotypes. We removed cultured cells from substrates by gentle trypsinization with 0.1% trypsin in PBS for 2 min. To select single cells, we plated cell suspensions into hydrogel microwell arrays containing no adhesive interface as previously described[23]. We picked single cells from arrays using a micromanipulator and then transferred them into a PCR lysis buffer. We performed nested RT-PCR as previously described[23], using the following primers: *Pax7* external, forward 5'-GAGTTCGATTAGCCGAGTGC-3', reverse 5'-GGTTAGCTCCTGCCTGCTTA-3'; *Pax7* internal, forward 5'-GCGAGAAGAAAGCCAAACAC-3', reverse 5'-GGGTGTAGATGTCCGGGTAG-3'; *Myf5* external, forward 5'-AGACGCCTGAAGAAGGTCAA-3', reverse 5'-AGCTGGACACGGAGCTTTTA-3'; *Myf5* internal, forward 5'-CCACCAACCCTAACCAGAGA-3', reverse 5'-CTGTTCTTTCGGGACCAGAC-3'; *Pax3* external, forward 5'-AACCATATCCGCCACAAGAT-3', reverse 5'-CTAGATCCGCCTCCTCCTCT-3'; *Pax3* Internal, forward 5'-CCCATGGTTGCGTCTCTAAG-3', reverse 5'-GGATGCGGCTGATAGAACTC-3'; *MyoD* external, forward 5'-TACCCAAGGTGGAGATCCTG-3', reverse 5'-GTGGAGATGCGCTCCACTAT-3'; *MyoD* internal, forward 5'-GCCTTCTACGCACCTGGAC-3', reverse 5'-ACTCTTCCCTGGCCTGGACT-3'; *Myog* external, forward 5'-GAAAGTGAATGAGGCCTTCG-3', reverse 5'-ACGATGGACGTAAGGGAGT-3'; *Myog* internal, forward 5'-CGGCTGCCTAAAGTGGAGAT-3', reverse 5'-GCAAATGATCTCCTGGGTTG-3'.

Hydrogel fabrication

We fabricated poly(ethylene glycol) (PEG) hydrogels from PEG precursors, synthesized as described previously[30]. Briefly, we formed hydrogels by mixing 10% (wt/vol) solutions of PEG-sulfhydryl (4-arm 10 kDa PEG-SH) and PEG-vinylsulfone (8-arm 10 kDa PEG-VS) precursor polymers diluted in water or triethanolamine, respectively. We functionalized hydrogel surfaces through covalent cross-linking reaction with PBS-dialyzed Laminin protein (Roche). We fabricated soft 12 kPa (Young's modulus) stiffness hydrogels to 1 mm thickness[30]. We fabricated rigid 10^6 kPa stiffness hydrogels to a 1–2 μm thickness directly onto tissue-culture plastic dishes[30]. Hydrogels of ≤1 μm thickness allow cells to sense the underlying substrate mechanical properties, resulting in an effective rigidity equivalent to tissue-culture plastic[30,55], while providing equivalent material surface chemistry as thicker, soft gels. This non-swelling gel chemistry results in equivalent laminin protein concentrations (estimated to be 7.5 ng cm^{-2} in[30]) on both soft and rigid hydrogels. We fabricated hydrogel microwell arrays for clonal proliferation experiments as described previously[30]. We cut and adhered all hydrogels to cover the surface area (2.0 cm^2) of 24-well culture plates.

MuSC culture, treatment, and lentiviral infection

Following isolation, we resuspened MuSCs in myogenic cell culture medium containing DMEM/F10 (50:50), 15% FBS, 2.5 ng ml^{-1} FGF-2 (bFGF), and 1% penicillin/streptomycin.

We seeded MuSC suspensions at a density of 1000 cells per well (2.0 cm^2 surface area). We maintained cell cultures at 37 °C in 5% CO_2 and changed media daily. For p38α/β inhibition studies, we added 0.05–25 μM SB202190 (EMD Chemicals) or 1 μM BIRB0796 (Axon MedChem) daily and compared these treatments with their solvent (DMSO, 0.1% final) control. We performed all MuSC cell culture assays and transplantations after one week of culture unless noted otherwise. For syngeneic transplant studies, we infected cultured MuSCs with EF1α promoter-driven *Luciferase*-IRES-*GFP* lentivirus, as described below.

$P16^{Ink4a}$ and $p21^{Cip1}$ immunocytometric analysis

We analyzed MuSCs from young or aged mice following FACS purification or after one week culture on 12 kPa hydrogels with exposure to 0.1% DMSO control or 10 μM SB202190. We collected cultured cells by incubation with 0.5% trypsin in PBS for 2 min at 37 °C. We cytopsun isolated cells to glass slides and fixed with 0.5% paraformaldehyde in PBS. We blocked fixed cells with 20% goat serum and 0.5% Triton X100 in PBS. We stained cells with mouse monoclonal anti-$p16^{Ink4a}$ IgG_{2a} (Santa Cruz Biotechnology, Santa Cruz, CA, catalog # 1661, 1:100) and rabbit anti-$p21^{Cip1}$ IgG (Abcam, Cambridge, MA, catalog # ab7960, 1:50) primary antibodies. To visualize primary antibody labelling, we stained cells with goat anti-mouse IgG AlexaFluor555-conjugated and goat anti-rabbit IgG AlexaFluor488-conjugated secondary antibodies (Invitrogen, 1:250 each). We counter-stained nuclei with Topro3 (Invitrogen). We acquired immunofluorescence images using a LSM510 laser-scanning confocal microscope (Carl Zeiss Microimaging) with a Plan NeoFluar 20×/0.75NA objective. We captured digital images using LSM510 software. We composed multi-panel images in Photoshop software (Adobe). We reduced background and enhanced contrast equivalently across all images of the same stain.

Phospho-flow cytometry

We assayed the phosphorylation of p38α/β MAPK and HSP27, readouts of p38 pathway activity, and cJun, a readout of JNK pathway activity, by phospho-flow cytometry. To assay phospho-p38α/β MAPK in freshly isolated MuSCs, we dissociated dissociated hindlimb skeletal muscles and then digested them for 90 min to isolate cells. We stained these cell suspensions for MuSC sorting markers (omitting propidium iodide) and then purified them by FACS as described above. We collected the sorted cells and immediately fixed them with 1.5% paraformaldehyde in PBS and then permeabilized them in methanol at –80 °C. We then washed the cells two times with staining buffer (0.5% BSA, 2.5 mM EDTA in PBS) and blocked them in staining buffer for 30 min at room temperature. We stained cells with a mouse anti-phospho (Thr180/Tyr182)-p38α/β MAPK IgG primary antibody (Cell Signaling Technology, catalog # 9216, 1:50) then a goat anti-mouse IgG AlexaFluor555-conjugated secondary antibody (Invitrogen, 1:250). We analyzed cells by gating again for $CD45^-CD31^-CD11b^-Sca1^-CD34^+\alpha7\text{-integrin}^+$ MuSCs and then analyzing these cells for phospho-p38α/β MAPK positivity on a modified FACStar Plus flow cytometer using FACS Diva software (BD Biosciences).

For culture studies, we maintained MuSCs on 12 kPa hydrogels and treated them daily with either 0.1% DMSO control or 10 μM SB202190. After seven days of culture, we collected cells by incubation with 0.5% trypsin in PBS for 2 min at 37 °C. We fixed and

permeabilized cells as described above and stained them with a rabbit anti-phospho (Ser82)-HSP27 (Cell Signaling, catalog # 2401, 1:100) or a rabbit anti-phospho (Ser63)-cJun (Cell Signaling, catalog # 9261, 1:100) primary antibody. Then, we stained cells with a donkey anti-rabbit AlexaFluor488-conjugated secondary antibody (Jackson ImmunoResearch Laboratories, 1:200). We washed cells twice with staining buffer and analyzed them on a FACSCalibur flow cytometer using the CellQuest software (both BD Biosciences).

Bulk proliferation assays

To assay bulk proliferation, we seeded MuSCs on flat hydrogels at a density of 1000 cells per 2.0 cm^2 surface area. After one week, we collected cells by incubation with 0.5% trypsin in PBS for 2 min at 37 °C and counted them using a hemocytometer.

Gene expression knockdown by siRNA treatment

To knock down p38α/β expression, we cultured aged MuSCs on collagen-coated tissue culture plastic for one day, collected them by incubation with 0.5% trypsin in PBS for 2 min at 37 °C and then transferred them to laminin-functionalized hydrogels for six more days. We transfected siRNA sequences (Ambion Silencer Select from Life Technologies, Carlsbad, CA) targeting p38α (*Mapk14*; ID: s77114) or p38β (*Mapk11*; ID: s72152) or scrambled control (100 nM; ID: negative control #2) at 100 nM once on the first day of culture using siIMPORTER reagents (Upstate, Charlottesville, VA). To test the specificity of individual siRNAs (each at 100 nM), we assayed the expression of p38α (*Mapk14*) and p38β (*Mapk11*) by RT-qPCR at day 3 post-treatment and compared to cells treated with the scramble control (100nM; Supplementary Fig. 4a,b). To test the efficacy of pooled p38α/β siRNAs (100nM each), we assayed the expression of p38α (*Mapk14*) and p38β (*Mapk11*) by RT-qPCR at day 5 post-treatment and compared to cells treated with the scramble control (200nM; Supplementary Fig. 4c,d). We also assayed phospho-HSP27, cell proliferation, and myogenic gene expression in cultured aged MuSCs treated with pooled 100 nM p38α/β siRNAs or 200 nM scrambled control (Fig. 3a–c, g, and h).

Clonal MuSC cell proliferation and fate analyses

We seeded MuSCs at a density of 500 cells per 2.0 cm^2 surface area hydrogel microwells with 600 μm diameter. This seeding density ensures that >90% of microwells contain a single cell. We monitored cell proliferation monitored by time-lapse microscopy from 12 h (day 0) to six days post-seeding and recorded images every 5 min at 10× magnification using a PALM/AxioObserver Z1 system (Carl Zeiss MicroImaging) with a custom environmental control chamber and motorized stage. We changed media every other day by ‘pausing’ the acquisition for <5 min. At the conclusion of the experiment, we fixed cells with 2% paraformaldehyde for 10 min and blocked them with 20% goat serum and 0.5% Triton X100 in PBS. We stained cells with a mouse monoclonal anti-myogenin antibody (BD Biosciences, catalog # 556358, 1:100) and then a donkey anti-mouse AlexaFluor555-conjugated secondary antibody (Invitrogen, 1:200). We counter-stained nuclei with Topro3 (Invitrogen). We acquired immunofluorescence images using a LSM510 laser-scanning confocal microscope (Carl Zeiss Microimaging) with a Plan NeoFluar 20×/0.75NA objective. We captured digital images using LSM510 software. We composed multi-panel

images in Photoshop software (Adobe). We reduced background and enhanced contrast equivalently across all images of the same stain. We analyzed time-lapse image sequences using the Baxter algorithm[30] in Matlab (Mathworks) to automatically identify and track single cells and generate hierarchical lineage trees.

Viable and dead cells were distinctly evident from time-lapse sequences due to phase contrast boundary and motility maintenance or loss, respectively. We determined the clonal viability percentage (Supplementary Fig. 3b) by relating the number of non-dividing clones that died during the long-term observation (by day 6) to the total number of viable clones observed on day 0. We determined the clonal division percentage (Figs. 2c and 3d) by relating the number of clones that divided at least once by day 6 to the total number of viable clones observed on day 0. We determined the total progeny of each clone from all viable cells within the dividing clone population (Fig. 4i). We determined the clonal differentiation percentage (Fig. 4i) by relating the number of Myogenin$^+$ cells to the total number of Topro3$^+$ positive cells at the culture endpoint in dividing clones.

Pax7 and Myogenin expression by flow cytometry

We isolated MuSCs from aged mice by FACS sorting and cultured them on 12 kPa hydrogels with either 0.1% DMSO control or 10 μM SB202190. After one week of culture, we collected cells by incubation with 0.5% trypsin in PBS for 2 min at 37 °C, fixed them in 1.5% paraformaldehyde and permeabilized them in methanol at −80°C. We then washed cells two times with staining buffer (0.5% BSA, 2.5 mM EDTA in PBS), and blocked them in staining buffer for 30 min at room temperature. We stained cells with rabbit polyclonal anti-Myogenin IgG (Santa Cruz Biotechnology, catalog # sc576, 1:100) and mouse anti-Pax7 IgG_1 (Santa Cruz Biotechnology, catalog # sc81648, 1:50) primary antibodies for 1 h at room temperature. Subsequently, we washed cells and incubated them with donkey anti-rabbit AlexaFluor488-conjugated and goat anti-mouse IgG_1 AlexaFluor647-conjugated secondary antibodies (Jackson ImmunoResearch Laboratories, 1:200 each) for 30 min at room temperature. We then washed cells twice with staining buffer and analyzed them on a FACSCalibur flow cytometer using CellQuest software (both BD Biosciences). In select studies (Fig. 3i), we combined anti-Pax7 and anti-phospho-HSP27 immunostaining analyses.

Quantitative real-time PCR

We isolated RNA from freshly isolated and cultured cells using the RNeasy Micro kit (Qiagen). We reverse transcribed cDNA from total mRNA from each sample using the High Capacity cDNA RT kit (Applied Biosystems). We subjected cDNA to real-time PCR using a SYBR Green PCR Master Mix (Applied Biosystems) in an ABI 7900HT Real Time PCR system and software (Applied Biosystems). We cycled samples at 95 °C for 10 min and then 40 cycles of 95 °C for 15 sec and 60 °C for 1 min. To quantify relative transcript levels, we used the $2^{-\Delta\Delta Ct}$ method to compare treated and untreated samples. *Gapdh* was used as a normalizing gene. We designed primer sequences for *Gapdh*[56], *Myog*, *Pax7*[57], *Mapk14* (p38α), *and Mapk11* (p38β) using NIH Primer3 or the cited report: *Gapdh*, forward 5'-CACTGAGCATCTCCCTCACA-3', reverse 5'-TGGGTGCAGCGAACTTTATT-3'; *Myog*, forward 5'-TGTTTGTAAAGCTGCCGTCTGA-3', reverse 5'-

CCTGCCTGTTCCCGGTATC-3'; *Pax7*, forward 5'-CTGGATGAGGGCTCAGATGT-3', reverse 5'-GGTTAGCTCCTGCCTGCTTA-3'; *Mapk14*, forward 5'-AAGACTCGTTGGAACCCCAG-3', reverse 5'-GGGTCGTGGTACTGAGCAAA-3'; *Mapk11*, forward 5'-TACCTCGTGACGACCCTGAT-3', reverse 5'-CGGTCATCTCCTCATCAGCC-3'.

Detection of donor-derived cells within the *in vivo* satellite cell niche and their response to injury

We collected the culture progeny of MuSCs from aged *Myf5*$^{nLacZ/+}$*/Luciferase* double-transgenic mice[23,43] by incubation with 0.1% trypsin in PBS for 2 min at 37 °C and transplanted them into *tibialis anterior* muscles of hindlimb-irradiated NOD/SCID mice. One month after transplant, we injected notexin to damage recipient muscles and activate MuSCs *in vivo*. Four days later, we collected, fixed, and cryosectioned recipient muscles, as described above. We performed immunohistological analysis of transverse tissue sections to detect β-galactosidase^{+} cells (indicating a donor-derived cell expressing Myf5, a marker of MuSC activation) in the satellite cell position within the myofiber basal lamina, as defined by laminin staining. We stained sections with anti-Laminin (Millipore, clone A5, catalog # 05-206, 1:250) and anti-β-galactosidase (Invitrogen, catalog # A11132, 1:100) primary antibodies and then with appropriate secondary antibodies (Invitrogen). We counter-stained nuclei with Hoechst 33342 (Invitrogen). We acquired images with an AxioPlan2 epi-fluorescent microscope (Carl Zeiss) with Plan NeoFluar 10×/0.30NA or 20×/0.75NA objectives (Carl Zeiss) and an ORCA-ER digital camera (Hamamatsu). We captured digital images in OpenLab software (Improvision) and assembled them using Photoshop software (Adobe) with consistent contrast adjustments across all images.

GFP transgene expression following lentiviral vector infection

We infected cultured MuSCs with a EF1α promoter-driven *Luciferase*-IRES-*GFP* lentivirus, generated as described previously[44,58]. We added lentivirus at 10,000 U ml^{-1} (10 MOI) in myogenic cell culture medium (1 ml per well) supplemented with 4 μg ml^{-1} protamine sulfate from 24 to 48 h post-seeding. We collected cultured cells at day 7 post-seeding by incubation with 0.5% trypsin in PBS for 2 min at 37 °C. We washed cells with 20% goat serum and 0.5% Triton X100 in PBS. We analyzed GFP expression (see Supplementary Fig. 8a) on a modified FACStar Plus flow cytometer using FACS Diva software (BD Biosciences).

In vivo force measurements

We performed force measurements on *tibialis anterior* (TA) muscles *in vivo* in anesthetized mice, as previously described[44,45]. We shaved hindlimbs and fixed them to a frame to immobilize it without compromising the blood supply to the leg. We warmed the animal on an isothermal pad and by heat lamp. We made a small incision in the skin directly above the TA muscle. We sutured the distal tendon to a thin metal hook and then attached to a 300C-LR force transducer (Aurora Scientific). We cut the distal tendons from all front lower hindlimb muscles other than TA, leaving the TA isolated during attachment to the force transducer. We kept the muscles and tendons moist by periodic wetting with saline (0.9%

sodium chloride) solution. We placed a bipolar electrical stimulation cuff around the central third of the TA. In all measurements, we used 0.1 ms pulses at predetermined supra-maximal stimulation intensity. For twitch force measurements, we stimulated the muscle with a single 0.1 ms pulse. For tetanic force measurements, we stimulated the muscle was stimulated at 150 Hz for 0.3 s. We recorded muscle force and synchronization pulses for 2 seconds immediately prior to the stimulation and 3 seconds after the end of the stimulation. We performed five twitch and then five tetanic measurements on each muscle, with 3–5 minutes between each measurement. We collected data with a PCI-6251 acquisition card (National Instruments) and analyzed it in Matlab. We calculated specific force values by normalizing the force measurements by the muscle physiological cross-sectional area (PCSA), as described previously[59]:

$$\mathrm{PCSA}=(\mathrm{muscle\ \ volume}/\mathrm{fiber\ \ length})\times(\cos\phi_{\mathrm{fibers}}). \quad \text{[eqn. 3]}$$

where $\varphi_{\mathrm{fibers}}$ is the pennation angle of the muscle fibers. We determined muscle volume by displacement and measured fiber length by micrometer.

Statistical analysis

We performed cell culture experiments with at least three replicates. For single-cell gene expression, proliferation, and immunofluorescence assays, we report the number of individual cells quantified in the legends. We used Fisher's exact tests in comparisons between conditions for single-cell assays and transplant engraftment frequencies. For transplant studies, we performed preliminary experiments then performed power-analyses of the Fischer's test prior to conducting our experiments in order to determine the lowest number of transplant recipients required to achieve statistical significance. In general, we performed primary transplant experiments in at least three independent experiments, with at least 15 total transplants per condition, unless otherwise noted. In some cases we powered our studies with unbalanced numbers of replicates (see Fig. 4b and Supplementary Fig. 1d) based on these power-analyses. We used unpaired, two-tailed *t* tests to compare between conditions for bulk and clonal proliferation, gene expression, flow cytometric, and force assays. We used a paired two-tailed *t* test to compare between conditions for serial transplant assays within shared cohorts of mice. W used unpaired, two-tailed Mann-Whitney tests to compare between conditions for myofiber counting and clone size and differentiation assays due to non-normality. We present box-and-whisker plots with a median central line, 50% CI box, and 95% CI whiskers. We used a significance level of $\alpha = 0.05$ for all tests.

Supplementary Material

Refer to Web version on PubMed Central for supplementary material.

ACKNOWLEDGMENTS

We would like to thank K. Koleckar, P. Kraft, N. Nguyen, A. Thayer, C. Marceau, K. Magnusson, and A. Ho for technical assistance; K. Havenstrite and R. Haynes for polymer synthesis; and the Stanford Center for Innovation in In-Vivo Imaging (SCI[3]), the Stanford Shared FACS Facility (SSFF), and IBM Almaden for technical support. This work was funded by US National Institutes of Health training grant R25CA118681 and grant K99AG042491 (B.D.C.); US National Institutes of Health training grant T32CA009151 and grant K99AR061465 and California Institute for Regenerative Medicine training grant TG2-01159 (P.M.G.); and US National Institutes of Health grants

U01HL100397, U01HL099997, R01AG020961, R01HL096113, and R01AG009521, IBM Faculty Award, California Institute for Regenerative Medicine grants RT1-01001 and TR3-05501, and the Baxter Foundation (H.M.B.).

REFERENCES

1. Ryall JG, Schertzer JD, Lynch GS. Cellular and molecular mechanisms underlying age-related skeletal muscle wasting and weakness. Biogerontology. 2008; 9:213–228. [PubMed: 18299960]
2. Grounds MD. Age-associated changes in the response of skeletal muscle cells to exercise and regeneration. Ann N Y Acad Sci. 1998; 854:78–91. [PubMed: 9928422]
3. Benny Klimek ME, et al. Acute inhibition of myostatin-family proteins preserves skeletal muscle in mouse models of cancer cachexia. Biochem Biophys Res Commun. 2010; 391:1548–1554. [PubMed: 20036643]
4. Di Marco S, et al. The translation inhibitor pateamine A prevents cachexia-induced muscle wasting in mice. Nat Commun. 2012; 3:896. [PubMed: 22692539]
5. Sandri M, et al. Foxo transcription factors induce the atrophy-related ubiquitin ligase atrogin-1 and cause skeletal muscle atrophy. Cell. 2004; 117:399–412. [PubMed: 15109499]
6. Stitt TN, et al. The IGF-1/PI3K/Akt pathway prevents expression of muscle atrophy-induced ubiquitin ligases by inhibiting FOXO transcription factors. Mol Cell. 2004; 14:395–403. [PubMed: 15125842]
7. Glass D, Roubenoff R. Recent advances in the biology and therapy of muscle wasting. Ann N Y Acad Sci. 2010; 1211:25–36. [PubMed: 21062293]
8. Sakuma K, Yamaguchi A. Molecular mechanisms in aging and current strategies to counteract sarcopenia. Curr Aging Sci. 2010; 3:90–101. [PubMed: 20158492]
9. Janssen I, Shepard DS, Katzmarzyk PT, Roubenoff R. The healthcare costs of sarcopenia in the United States. J Am Geriatr Soc. 2004; 52:80–85. [PubMed: 14687319]
10. Mauro A. Satellite cell of skeletal muscle fibers. J Biophys Biochem Cytol. 1961; 9:493–495. [PubMed: 13768451]
11. Brack AS, Rando TA. Intrinsic changes and extrinsic influences of myogenic stem cell function during aging. Stem Cell Rev. 2007; 3:226–237. [PubMed: 17917136]
12. Gopinath SD, Rando TA. Stem cell review series: aging of the skeletal muscle stem cell niche. Aging Cell. 2008; 7:590–598. [PubMed: 18462272]
13. Brack AS, et al. Increased Wnt signaling during aging alters muscle stem cell fate and increases fibrosis. Science. 2007; 317:807–810. [PubMed: 17690295]
14. Conboy IM, Conboy MJ, Smythe GM, Rando TA. Notch-mediated restoration of regenerative potential to aged muscle. Science. 2003; 302:1575–1577. [PubMed: 14645852]
15. Conboy IM, et al. Rejuvenation of aged progenitor cells by exposure to a young systemic environment. Nature. 2005; 433:760–764. [PubMed: 15716955]
16. Collins CA, Zammit PS, Ruiz AP, Morgan JE, Partridge TA. A population of myogenic stem cells that survives skeletal muscle aging. Stem Cells. 2007; 25:885–894. [PubMed: 17218401]
17. Chakkalakal JV, Jones KM, Basson MA, Brack AS. The aged niche disrupts muscle stem cell quiescence. Nature. 2012; 490:355–360. [PubMed: 23023126]
18. Cerletti M, et al. Highly efficient, functional engraftment of skeletal muscle stem cells in dystrophic muscles. Cell. 2008; 134:37–47. [PubMed: 18614009]
19. Kuang S, Kuroda K, Le Grand F, Rudnicki MA. Asymmetric self-renewal and commitment of satellite stem cells in muscle. Cell. 2007; 129:999–1010. [PubMed: 17540178]
20. Montarras D, et al. Direct isolation of satellite cells for skeletal muscle regeneration. Science. 2005; 309:2064–2067. [PubMed: 16141372]
21. Cornelison DD, et al. Essential and separable roles for Syndecan-3 and Syndecan-4 in skeletal muscle development and regeneration. Genes Dev. 2004; 18:2231–2236. [PubMed: 15371336]
22. Bosnakovski D, et al. Prospective isolation of skeletal muscle stem cells with a Pax7 reporter. Stem Cells. 2008; 26:3194–3204. [PubMed: 18802040]

23. Sacco A, Doyonnas R, Kraft P, Vitorovic S, Blau HM. Self-renewal and expansion of single transplanted muscle stem cells. Nature. 2008; 456:502–506. [PubMed: 18806774]
24. Lefkovits, I.; Waldmann, H. Limiting dilution analysis of cells of the immune system. Oxford: Oxford Univ. Press; 1999.
25. Rocheteau P, Gayraud-Morel B, Siegl-Cachedenier I, Blasco MA, Tajbakhsh S. A subpopulation of adult skeletal muscle stem cells retains all template DNA strands after cell division. Cell. 2012; 148:112–125. [PubMed: 22265406]
26. Darabi R, et al. Assessment of the myogenic stem cell compartment following transplantation of Pax3/Pax7-induced embryonic stem cell-derived progenitors. Stem Cells. 2011; 29:777–790. [PubMed: 21374762]
27. Rossi DJ, Jamieson CH, Weissman IL. Stems cells and the pathways to aging and cancer. Cell. 2008; 132:681–696. [PubMed: 18295583]
28. Seale P, et al. Pax7 is required for the specification of myogenic satellite cells. Cell. 2000; 102:777–786. [PubMed: 11030621]
29. Kang JS, Krauss RS. Muscle stem cells in developmental and regenerative myogenesis. Curr Opin Clin Nutr Metab Care. 2010; 13:243–248. [PubMed: 20098319]
30. Gilbert PM, et al. Substrate elasticity regulates skeletal muscle stem cell self-renewal in culture. Science. 2010; 329:1078–1081. [PubMed: 20647425]
31. Cosgrove BD, Sacco A, Gilbert PM, Blau HM. A home away from home: challenges and opportunities in engineering in vitro muscle satellite cell niches. Differentiation. 2009; 78:185–194. [PubMed: 19751902]
32. Shefer G, Van de Mark DP, Richardson JB, Yablonka-Reuveni Z. Satellite-cell pool size does matter: defining the myogenic potency of aging skeletal muscle. Dev Biol. 2006; 294:50–66. [PubMed: 16554047]
33. Schultz E, Lipton BH. Skeletal muscle satellite cells: changes in proliferation potential as a function of age. Mech Ageing Dev. 1982; 20:377–383. [PubMed: 7166986]
34. Mouly V, et al. The mitotic clock in skeletal muscle regeneration, disease and cell mediated gene therapy. Acta Physiol Scand. 2005; 184:3–15. [PubMed: 15847639]
35. Garcia-Prat L, Sousa-Victor P, Munoz-Canoves P. Functional dysregulation of stem cells during aging: a focus on skeletal muscle stem cells. Febs J. 2013; 280:4051–4062. [PubMed: 23452120]
36. Beccafico S, et al. Human muscle satellite cells show age-related differential expression of S100B protein and RAGE. Age (Dordr). 2011; 33:523–541. [PubMed: 21140295]
37. Wong ES, et al. p38MAPK controls expression of multiple cell cycle inhibitors and islet proliferation with advancing age. Dev Cell. 2009; 17:142–149. [PubMed: 19619499]
38. Ito K, et al. Reactive oxygen species act through p38 MAPK to limit the lifespan of hematopoietic stem cells. Nat Med. 2006; 12:446–451. [PubMed: 16565722]
39. Iwasa H, Han J, Ishikawa F. Mitogen-activated protein kinase p38 defines the common senescence-signalling pathway. Genes Cells. 2003; 8:131–144. [PubMed: 12581156]
40. Bain J, et al. The selectivity of protein kinase inhibitors: a further update. Biochem J. 2007; 408:297–315. [PubMed: 17850214]
41. Jones NC, et al. The p38alpha/beta MAPK functions as a molecular switch to activate the quiescent satellite cell. The Journal of cell biology. 2005; 169:105–116. [PubMed: 15824134]
42. Troy A, et al. Coordination of satellite cell activation and self-renewal by Par-complex-dependent asymmetric activation of p38alpha/beta MAPK. Cell Stem Cell. 2012; 11:541–553. [PubMed: 23040480]
43. Tajbakhsh S, et al. Gene targeting the myf-5 locus with nlacZ reveals expression of this myogenic factor in mature skeletal muscle fibres as well as early embryonic muscle. Dev Dyn. 1996; 206:291–300. [PubMed: 8896984]
44. Sacco A, et al. Short telomeres and stem cell exhaustion model Duchenne muscular dystrophy in mdx/mTR mice. Cell. 2010; 143:1059–1071. [PubMed: 21145579]
45. Llewellyn ME, Thompson KR, Deisseroth K, Delp SL. Orderly recruitment of motor units under optical control in vivo. Nat Med. 2010; 16 1161-U1144.

46. Thompson LV. Effects of age and training on skeletal muscle physiology and performance. Phys Ther. 1994; 74:71–81. [PubMed: 8265730]
47. Arpke RW, et al. A New Immuno-, Dystrophin-Deficient Model, the NSG-mdx(4Cv) Mouse, Provides Evidence for Functional Improvement Following Allogeneic Satellite Cell Transplantation. Stem Cells. 2013; 31:1611–1620. [PubMed: 23606600]
48. Lluis F, Perdiguero E, Nebreda AR, Munoz-Canoves P. Regulation of skeletal muscle gene expression by p38 MAP kinases. Trends Cell Biol. 2006; 16:36–44. [PubMed: 16325404]
49. Palacios D, et al. TNF/p38alpha/polycomb signaling to Pax7 locus in satellite cells links inflammation to the epigenetic control of muscle regeneration. Cell Stem Cell. 2010; 7:455–469. [PubMed: 20887952]
50. Brien P, Pugazhendhi D, Woodhouse S, Oxley D, Pell JM. p38alpha MAPK regulates adult muscle stem cell fate by restricting progenitor proliferation during postnatal growth and repair. Stem Cells. 2013; 31:1597–1610. [PubMed: 23592450]
51. Tivey HS, et al. Small molecule inhibition of p38 MAP kinase extends the replicative life span of human ATR-Seckel syndrome fibroblasts. J Gerontol A Biol Sci Med Sci. 2013; 68:1001–1009. [PubMed: 23401567]
52. Zou J, et al. Inhibition of p38 MAPK activity promotes ex vivo expansion of human cord blood hematopoietic stem cells. Ann Hematol. 2012; 91:813–823. [PubMed: 22258328]
53. Parham DM, Ellison DA. Rhabdomyosarcomas in adults and children: an update. Arch Pathol Lab Med. 2006; 130:1454–1465. [PubMed: 17090187]
54. Page TH, Brown A, Timms EM, Foxwell BM, Ray KP. Inhibitors of p38 suppress cytokine production in rheumatoid arthritis synovial membranes: does variable inhibition of interleukin-6 production limit effectiveness in vivo? Arthritis Rheum. 62:3221–3231. [PubMed: 20589681]
55. Engler AJ, Sen S, Sweeney HL, Discher DE. Matrix elasticity directs stem cell lineage specification. Cell. 2006; 126:677–689. [PubMed: 16923388]
56. Pajcini KV, Corbel SY, Sage J, Pomerantz JH, Blau HM. Transient inactivation of Rb and ARF yields regenerative cells from postmitotic mammalian muscle. Cell Stem Cell. 2010; 7:198–213. [PubMed: 20682446]
57. Le Grand F, Jones AE, Seale V, Scime A, Rudnicki MA. Wnt7a activates the planar cell polarity pathway to drive the symmetric expansion of satellite stem cells. Cell Stem Cell. 2009; 4:535–547. [PubMed: 19497282]
58. Westerman KA, Ao ZJ, Cohen EA, Leboulch P. Design of a trans protease lentiviral packaging system that produces high titer virus. Retrovirology. 2007; 4
59. Sacks RD, Roy RR. Architecture of the hindlimb muscles of cats: functional significance. J Morphol. 1982; 173:185–195. [PubMed: 7120421]

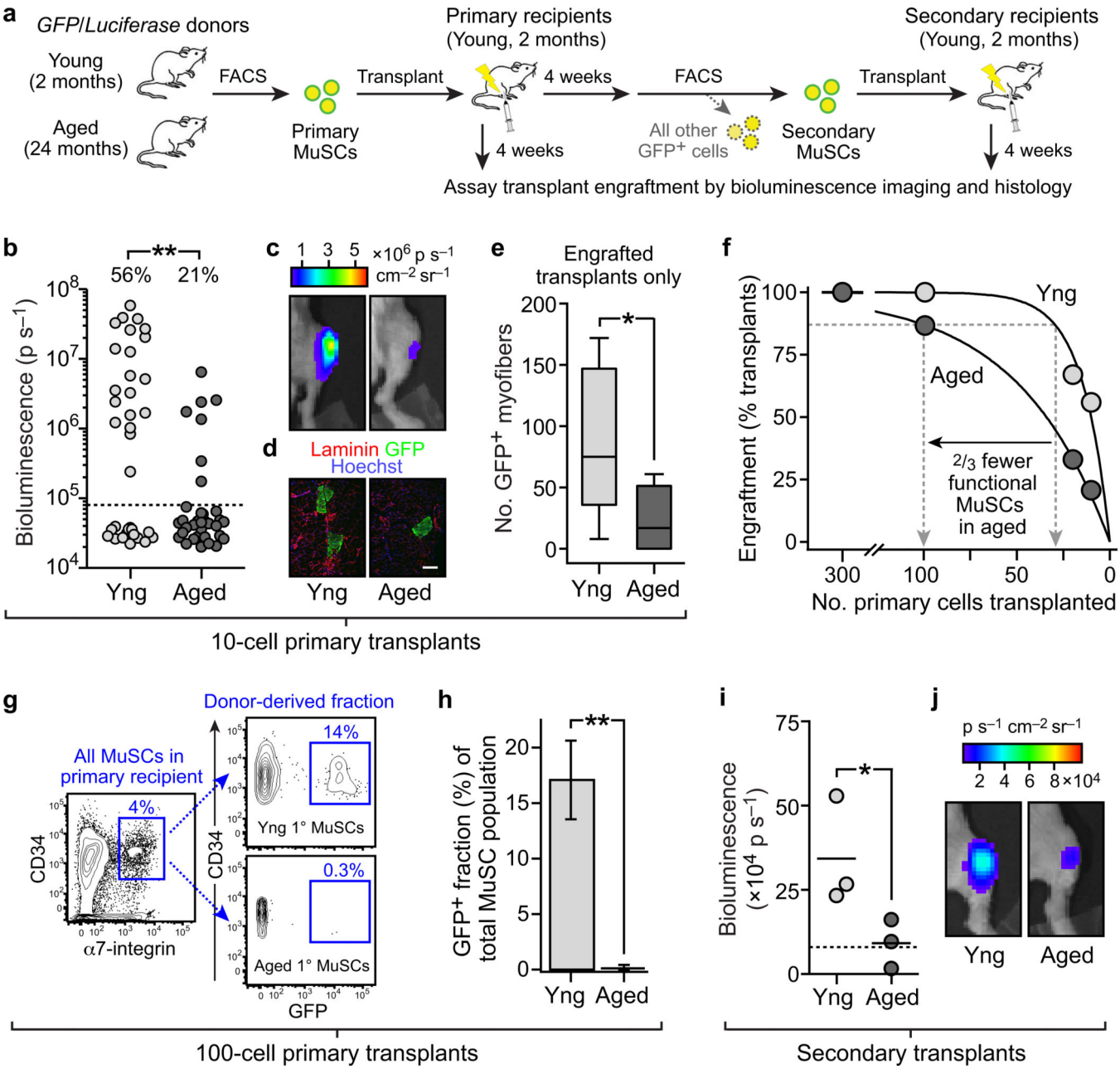

Figure 1. Aged MuSCs have diminished regenerative and self-renewal functions revealing an inherent stem cell defect

(**a**) MuSC intramuscular transplantation scheme. (**b–e**) Bioluminescence imaging (BLI) and immunohistology of 10-cell primary transplants from young (Yng) or aged *GFP/Luciferase* MuSC donors. (**b**) BLI signals from $n = 34$ recipients from three experiments. p, photons. Engraftment threshold (dashed line) corresponding to histological detection of ≥1 donor-derived (GFP^+) myofibers in (**b**) and (**i**). Representative BLI (**c**) and immunohistological (**d**) images. Scale bar, 500 μm. (**e**) GFP^+ myofibers per recipient tibialis anterior muscle ($n = 6$–7 recipients from three experiments) in engrafted samples. (**f**) Limiting dilution analysis relating primary MuSCs transplanted with percent engraftment from $n = 5$–34 transplants

per condition. (**g**, **h**) Flow cytometric analysis of GFP^+ fraction of all $CD34^+\alpha7\text{-integrin}^+$ MuSCs in primary recipients ($n = 3$, mean ± s.e.m.) transplanted with 100 primary (1°) young or aged MuSCs. (**i**, **j**) BLI analysis of secondary recipients transplanted with re-isolated $GFP^+CD34^+\alpha7\text{-integrin}^+$ cells from 700 primary young or aged MuSC recipients. (**i**) BLI scatter plot (mean overlaid, $n = 3$). (**j**) Representative BLI images. $P < 0.05$ (*) or $P < 0.01$ (**) by Fisher's exact test in (**b**), Mann-Whitney test in (**e**), unpaired *t* test in (**h**), and paired *t* test in (**i**).

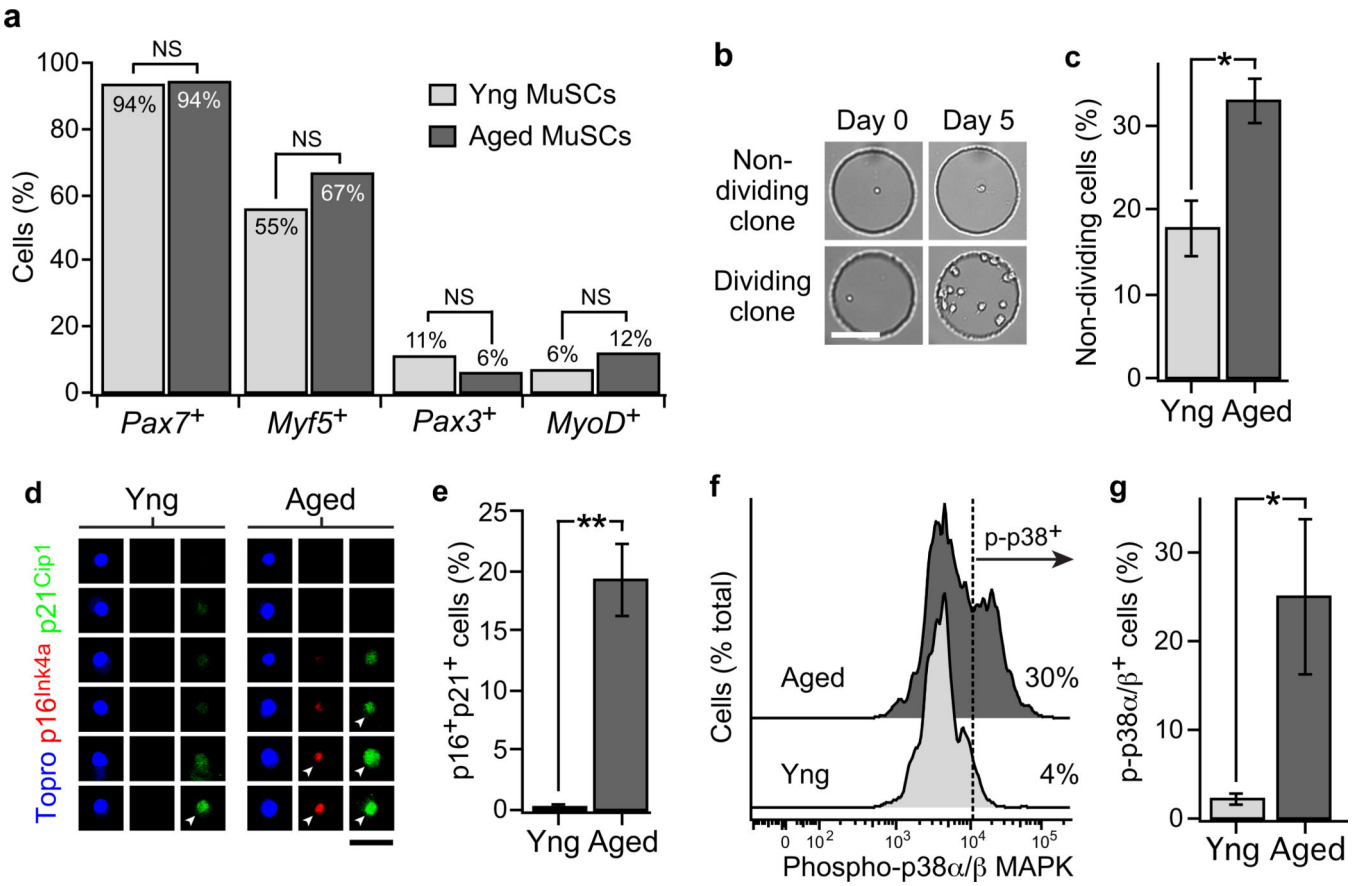

Figure 2. Aged MuSCs are characterized by a senescence phenotype and elevated p38α/β MAPK signaling

(**a**) Single-cell RT-PCR analysis of muscle stem cell (*Pax7* and *Myf5*) and myogenic commitment gene (*Pax3* and *MyoD*) expression in purified young (Yng) or aged MuSCs (*n* = 47 and 33 cells, respectively, from two experiments). (**b**, **c**) Clonal division assay. (**b**) Representative brightfield images of non-dividing and dividing clones. Scale bar, 100 μm. (**c**) Proportion of young or aged MuSCs that do not undergo clonal division in hydrogel microwell cultures (mean ± s.e.m. of *n* = 4 experiments). (**d**, **e**) Immunostaining analysis of $p16^{Ink4a}$ and $p21^{Cip1}$ senescence marker expression in purified young and aged MuSCs, with Topro3 nuclear counter-staining. (**d**) Six representative cells per condition. Positive cells marked with arrowheads. Scale bar, 10 μm. (**e**) Fraction expressing both $p16^{Ink4a}$ and $p21^{Cip1}$ (mean ± s.e.m. of *n* = 3 experiments). (**f**, **g**) Flow cytometric analysis of phospho-p38α/β MAPK in purified young or aged MuSCs. (**f**) Representative histograms. (**g**) Mean ± s.e.m. of *n* = 3 experiments. Not significant (NS), $P < 0.05$ (*) or $P < 0.01$ (**) by Fisher's exact test in (**a**) and Student's *t* test in (**c**, **e**, **g**).

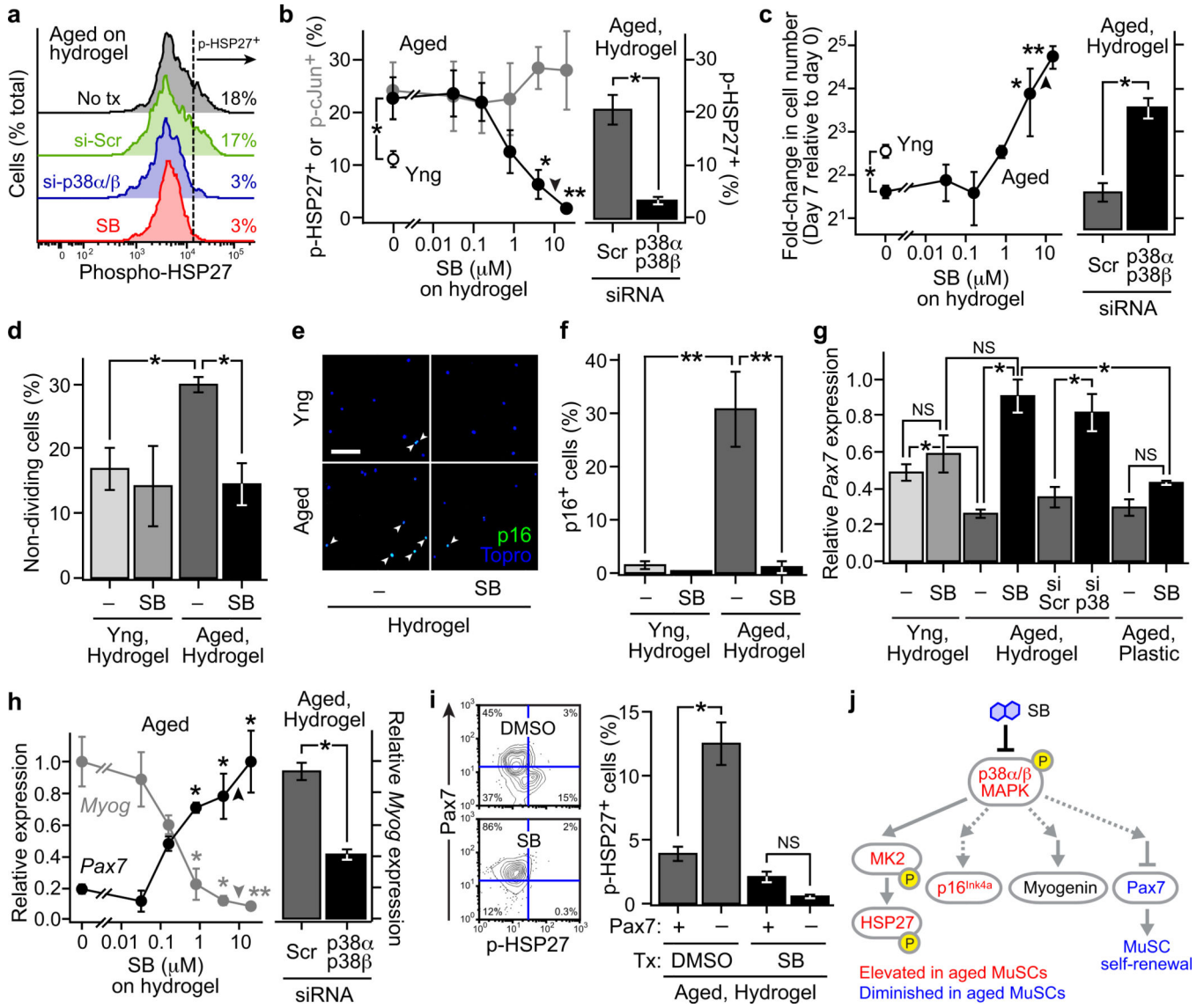

Figure 3. p38α/β MAPK inhibition induces proliferation and augments stem-cell gene expression in aged MuSCs in soft hydrogel cultures

(**a**–**i**) Analyses of young (Yng) or aged MuSCs after culture on plastic or soft hydrogels with the p38α/β inhibitor SB202190 (SB; 10 μM unless noted) or DMSO control (–), or with an siRNA pool targeting p38α and p38β or a scrambled control (Scr). Arrowheads denote 10 μM in (**b**, **c**, **h**). (**a**, **b**) HSP27 and cJun phosphoprotein flow cytometry analyses. (**a**) Representative phospho-HSP27 histograms. (**b**) Fraction of phospho-HSP27 or phospho-cJun positive cells (mean ± s.e.m. of $n = 3$ culture replicates from one experiment. (**c**) Bulk proliferation analyses (mean ± s.e.m. from $n = 3$–6 culture replicates from one experiment). (**d**) Clonal division analysis (mean ± s.e.m. of $n = 4$ experiments). (**e**, **f**) $p16^{Ink4a}$ immunostaining analysis. (**e**) Representative images. Arrowheads, positive cells. Scale bar, 100 μm. (**f**) Fraction of cells expressing $p16^{Ink4a}$ (mean ± s.e.m. of $n = 4$ culture replicates). (**g**, **h**) RT-qPCR analysis of *Pax7* and *Myogenin* expression. (**g**) Mean ± s.e.m of $n = 6$ culture replicates from two experiments. (**h**) Mean ± s.e.m of $n = 3$ culture replicates from

one experiment. (**i**) Flow cytometric analysis of Pax7 and phospho-HSP27. Left, representative scatter plots. Right, p-HSP27^{+} incidence in Pax7$^{+/-}$ fractions (mean ± s.e.m of $n = 3$ culture replicates from one experiment). Not significant (NS), $P < 0.05$ (*) or $P < 0.01$ (**) for conditions different than control by *t* test in (**b**–**d**, **f**–**i**). (**j**) Summary of SB effects on aged MuSCs in hydrogel cultures.

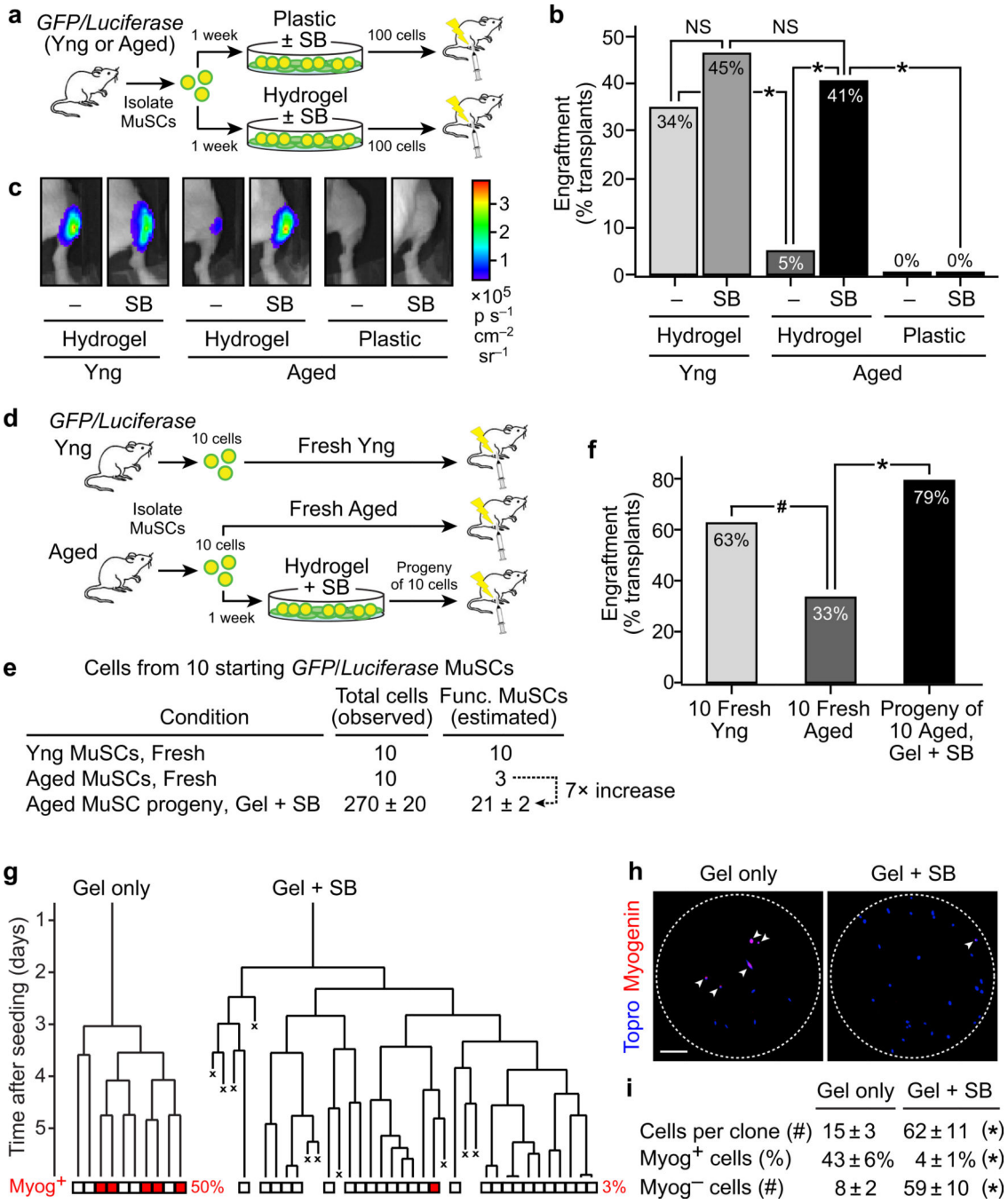

Figure 4. p38α/β inhibition and soft hydrogel substrate synergistically increase the total yield of functional aged stem cells

(**a**–**c**) Engraftment analysis of 100-cell transplants of young (Yng) or aged *GFP*/*Luciferase* MuSC population after culture on plastic or hydrogel with SB202190 (SB; 10 μM) or DMSO control (–) into NOD/SCID hindlimbs by bioluminescence imaging (BLI). (**a**) Transplantation scheme. (**b**) Percentage of transplants above engraftment threshold (n = 41, 44, 63, 32, 10, and 10 per condition from three experiments). (**c**) Representative BLI images. p, photons. (**d**–**f**) Engraftment analysis of transplants of the total cell yield of 10 aged

MuSCs after SB/hydrogel culture or 10 young or 10 aged freshly isolated MuSCs. (**d**) Transplant scheme. (**e**) Estimated number of functional MuSCs per condition based *GFP*/*Luciferase* MuSC proliferation in culture (n = 3, mean ± s.e.m) and functional MuSC frequencies calculated in Supplementary Fig. 7b. (**f**) Percentage of transplants above engraftment threshold (n = 24 from one experiment). (**g**) Representative fate trees for single aged MuSCs in hydrogel culture without or with SB treatment (n = 64 and 75 clones from two experiments). 'X' indicates cell death. (**h**) Corresponding Myogenin (Myog) immunostaining images. Arrowheads, positive nuclei. Scale bar, 100 μm. Microwell boundary, dashed line. (**i**) Total and Myogenin$^-$ cell numbers and percentage of Myogenin$^+$ cells per dividing clone (median ± s.e.m). Not significant (NS), P = 0.08 (#) or P < 0.05 (*) by Fisher's exact test in (**b**) and (**f**) or Mann-Whitney test in (**i**).

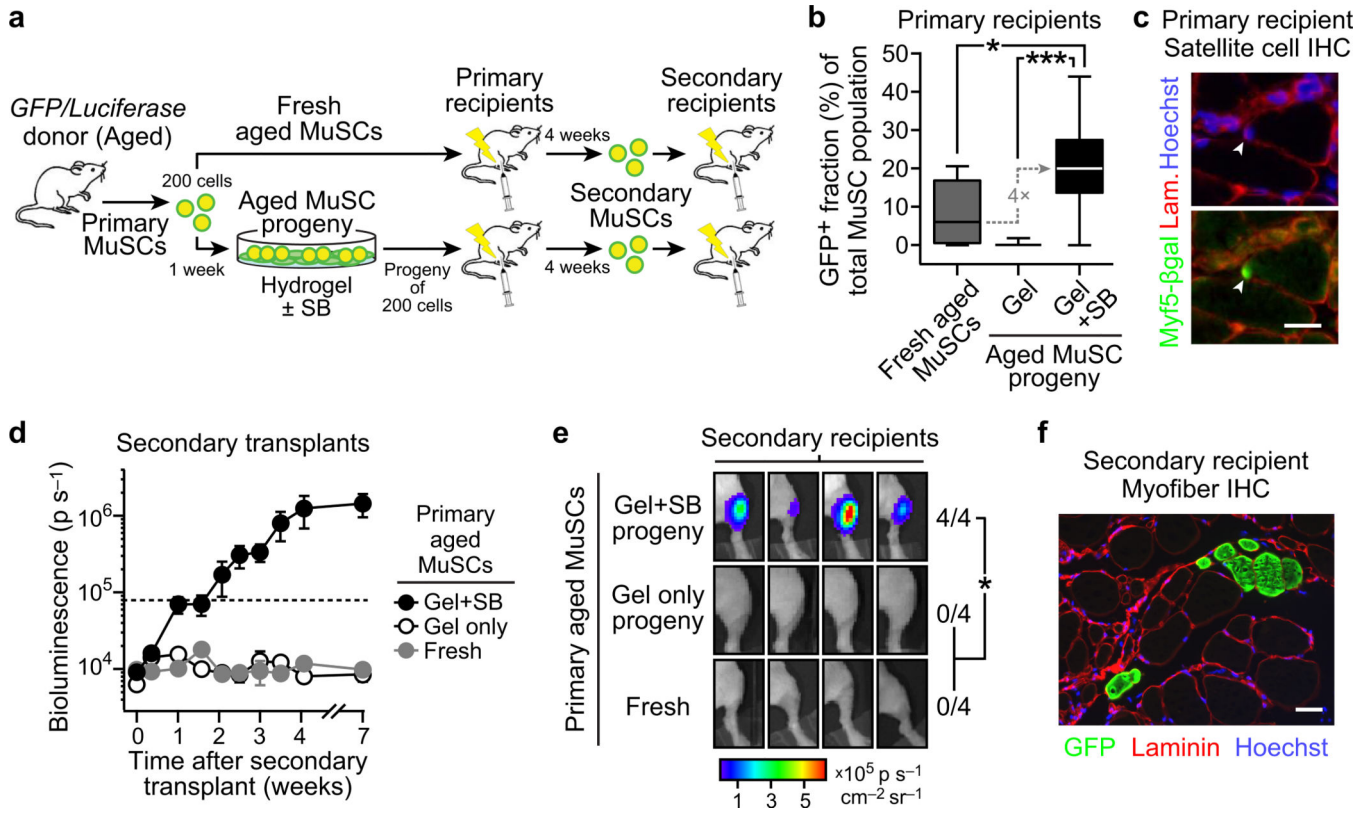

Figure 5. ***Ex vivo*-expanded aged MuSC progeny reconstitute the stem cell reserve *in vivo* and serially transplant**

(**a**, **b**, **d–f**) Analyses of stem cell repopulation in primary recipients and transplant engraftment in secondary recipients comparing 200 freshly isolated aged *GFP/Luciferase* MuSCs and the progeny of 200 aged MuSCs after culture on hydrogel ± SB202190 (SB; 10 μM). (**a**) Serial transplant scheme. (**b**) Frequency of donor-derived (GFP^+) cells in the $CD34^+\alpha7\text{-integrin}^+$ MuSC population in primary recipient muscles (n = 8–10 per condition). Box-and-whisker plot with median line. (**c**) Immunohistochemical (IHC) analysis of representative transverse section from notexin-injured muscles transplanted with the progeny of 100 aged *Myf5*$^{nLacZ/+}$ MuSCs after culture on hydrogel with 10 μM SB. Arrowhead indicates Myf5–β-gal^+ cell in satellite position. Scale bar, 50 μm. (**d–f**) Engraftment analysis of secondary transplant recipients (n = 4). (**d**) BLI signals for up to 2 months after transplant (mean ± s.e.m.). Dashed line represents engraftment detection threshold. p, photons. (**e**) Representative BLI images at 4 weeks. Engraftment ratios are noted. (**f**) GFP immunohistochemistry (IHC) of transverse section from representative secondary recipient of SB/hydrogel aged MuSC progeny primary transplant. Scale bar, 75 μm. $P < 0.05$ (*) or $P < 0.001$ (***) by unpaired t test in (**b**) or Fisher's exact test in (**e**).

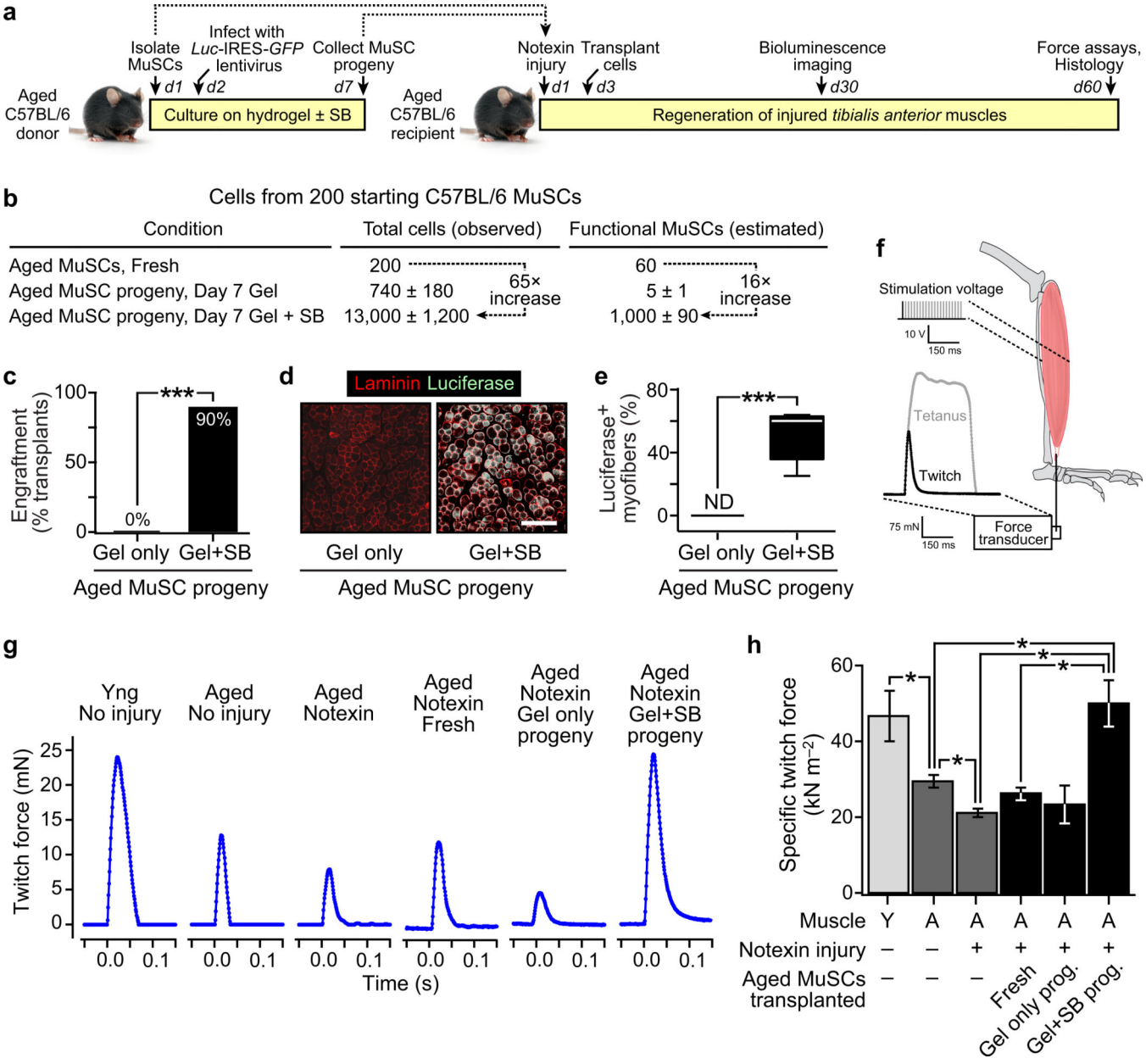

Figure 6. Restoration of muscle strength in injured aged mice by transplantation of *ex vivo*-expanded aged MuSC progeny

(**a–e**) Engraftment analysis of 200 fresh C57BL/6 aged MuSC or their progeny after culture on hydrogel ± SB202190 (SB; 10 μM) transplanted into syngeneic injured aged recipient muscles. (**a**) Transplant scheme. (**b**) Estimated number of functional MuSCs per condition based C57BL/6 MuSC proliferation in culture (n = 3, mean ± s.e.m) and functional MuSC frequencies calculated in Supplementary Fig. 7b. (**c**) Transplant engraftment frequency from bioluminescence imaging (n = 10 recipients from two experiments). (**d–e**) Luciferase immunohistochemistry in transverse muscle sections. (**d**) Representative images. Scale bar, 500 μm. (**e**) Box-and-whisker plot with median line of percent Luciferase$^+$ myofibers (n = 7 per condition). ND, none detected. (**f**) *In vivo* muscle contractile force assay scheme. (**g**)

Representative raw muscle twitch forces in young (Y) and aged (A) mice, without (−) or with (+) notexin injury and subsequent aged MuSC transplantation. (**h**) Specific muscle twitch forces (mean ± s.e.m. of $n = 5$ muscles per condition). $P < 0.05$ (*) or $P < 0.001$ (***) by Fisher's exact test in (**c**), Mann-Whitney test in (**e**), or *t* test in (**h**).